Acta Mech 226, 3205–3219 (2015)
DOI 10.1007/s00707-015-1365-8

ORIGINAL PAPER

Juan Yang · Xing Li

The scattering of the SH wave on a limited permeable crack in a functionally graded piezoelectric substrate bonded to a homogeneous piezoelectric strip

Received: 15 December 2014 / Revised: 12 February 2015 / Published online: 14 May 2015

Abstract The scattering problem of the SH wave on a limited permeable crack in a functionally graded piezoelectric substrate bonded to a homogeneous piezoelectric strip is investigated. We adopted the limited permeable crack surface boundary condition. By using the Fourier cosine transform, this mixed boundary value problem is reduced to two pairs of dual integral equations, which are solved numerically by the Copson method. Numerical results showed the effects of gradient parameter, electric loading, electric boundary conditions, incident angle, thickness of PM strip, the distance from the crack to the interface, and wave number on the dynamic stress intensity factor.

1 Introduction

Piezoelectric materials (PMs) exhibit practically useful phenomena because they produce an electric field when being deformed and undergo deformation when subjected to an electric field. Due to this intrinsic electromechanical coupling behavior, piezoelectric materials have been widely used in modern technologies as sensors and actuators, being often adhered to substrates or embedded in polymer matrices. However, smart piezoelectric materials tend to fracture during manufacturing and under in-service loading conditions because of their brittleness in nature. To satisfy the demand of advanced PMs in lifetime and reliability, the concept of functionally graded materials (FGMs) has recently been extended into the PMs with the help of the development in modern material processing technology. Such a gradient can be obtained from a resistivity nonuniformity introduced into the PZT ceramic, and it can be made possible by doping with small amounts of various additives, or by stacking piezoelectric composites of different compositions on top of each other. Therefore, it is necessary to study the electroelastic interaction and fracture behavior of these materials, and the problems on fracture mechanics of piezoelectric materials, and the functionally graded piezoelectric materials have attracted substantial attention in the scientific literature [1–11].

The study of scattering of elastic waves by subsurface defects has been the focus of interest of many recent researches due to its relevance to problems in nondestructive evaluation and material characterizations. Shen and Kuang [12] investigated the elastic wave scattering from an interface crack in laminated anisotropic media and in a layered half-space. Wang and Meguid [13] solved the interaction of SH wave with some cracks in a piezoelectric material by using integral transform and Chebyshev polynomials. Gu et al. [14] discussed the elastic wave scattering by an interface crack between a piezoelectric layer and an elastic substrate. Ueda [15]

J. Yang · X. Li (✉)
School of Mathematics and Computer Science, Ningxia University, No. 489, Helanshan Road, Yinchuan 750021, Ningxia, People's Republic of China
E-mail: li_x@nxu.edu.cn

J. Yang
E-mail: yj8024548@163.com

studied the diffraction of anti-plane shear waves in a piezoelectric laminated material with a vertical crack by the integral transform and the singular integral equation methods. Zhou and Wang [16] discussed the scattering of harmonic anti-plane shear waves by an interface crack in magneto-electro-elastic composites by using integral transform and Schmidt method. The scattering problem of an elastic wave by two collinear cracks in a functionally graded interlayer bonded to a dissimilar half-plane under anti-plane shear was analyzed by Ma et al. [17]. Li and Liu [18] considered scattering of the SH wave from a crack in a piezoelectric substrate bonded to a half-space of FGMs by Fourier integral transform and singular integral equation method, respectively. Huang and Li [19] studied the propagation of shear waves along a weak interface of two dissimilar magneto-electric or magneto-electro-elastic materials. The characteristics of wave propagation in structures with a single piezoelectric layer and periodic piezoelectric layers were also considered by Zhao et al. [20]. Propagation of SH waves in layered functionally gradient piezoelectric–piezomagnetic structures was analyzed by Singh and Rokne [21]. Using Fourier integral transform and the Copson method, Yang and Li [22] studied the scattering of the SH wave by a crack magneto-electro-elastic material substrate bonded to a piezoelectric material. The main attention was paid to the contact zone model, and some simplified (permeable and impermeable) electric boundary conditions were used.

For a slit crack, since the dielectric constant of a piezoceramic is much higher than that of the air (or vacuum) filling the crack, the electric boundary condition may be very sensitive to the crack opening or sliding caused by the applied mechanical and electric loads. Strictly, even if the permittivity of air is quite small, the flux of an electric field through the crack gap should not be zero, so it is better to take the electric boundary condition in the following form [23], $D_2^+ = D_2^-;\ D_2^+(u_2^+ - u_2^-) = -\varepsilon_a(\varphi^+ - \varphi^-)$, in which $D_i, \varphi, \varepsilon_a$ and $(u_2^+ - u_2^-)$ are the electric displacement component along the x_2-axis, the electric potential, permittivity of air in the crack, and the opening displacement component of crack surfaces. This electric boundary condition was first given in Hao's paper [23] and will be reduced to the permeable boundary condition when $u_2^+ - u_2^- = 0$ and to the impermeable one when $\varepsilon_a = 0$. In the previous studies, the limited permeable crack face boundary conditions [24,25] were applied to study the problem for scattering of the SH. Although many results have been obtained for scattering of elastic waves, the scattering of the SH wave on a crack has an arbitrary incidence angle, which is much closer to the actual situation, but most of the articles mentioned before assumed that the elastic wave incidents vertically, which is different from the actual situation. In addition, the Copson method other than singular integral equation method is applied to address the crack problem, which may be proven to be a robust way of solving the fracture problem of smart materials. An attempt has been made to apply this method to analyze the electroelastic dynamic behavior of a piezoelectric material. Moreover, smart devices are usually made up of layered multiferroic materials. Thus, the structure with a functionally graded piezoelectric substrate bonded to a homogeneous piezoelectric strip is considered. It is with this in mind that the scattering of the SH wave with an incidence angle θ on a limited permeable crack in a functionally graded substrate bonded to a homogeneous piezoelectric strip is investigated using the Fourier cosine transform and the Copson method [26]. In the analysis, we consider the limited permeable crack boundary condition.

In this paper, we use the Fourier transform and the Copson method to investigate the problem for scattering of the SH wave on a limited permeable crack in a functionally graded piezoelectric substrate bonded to a homogeneous piezoelectric strip. The analysis has been conducted on the electrically limited permeable crack boundary condition [24,25] described in Sect. 3. The material properties are assumed in exponential forms. By using integral transform techniques, the problem is first reduced to two pairs of dual integral equations and then into Fredholm integral equations of the second kind. The numerical results showed the effects of the gradient parameter, electric loading, electric boundary condition, the angle of wave, the distance from the crack to the interface, thickness of PM, and wave number upon the normalized dynamic stress intensity factor (NDSIF).

2 Formulation of the problem

Consider a crack of length $2a$ in an FGPM substrate bonded to a homogeneous piezoelectric strip with thickness h_3 in Fig. 1. The distance between the crack and the bonded interface is denoted by h_2. The crack is referred to the Cartesian coordinate system (x, y, z) with the origin located at the center of the crack. For convenience, it is assumed that the FGPM consists of upper ($y > 0$, thickness h_2) and lower ($y < 0$) regions. Quantities in the FGPS and the PM will subsequently be designated by subscripts k(=1, 2 and 3, respectively). Also, subscripts $k = 1$ and $k = 2$ indicate lower and upper regions of the FGPM, respectively, hereafter. Since the poling directions of piezoelectric materials are orientated along the z-axis, the anti-plane mechanical field and

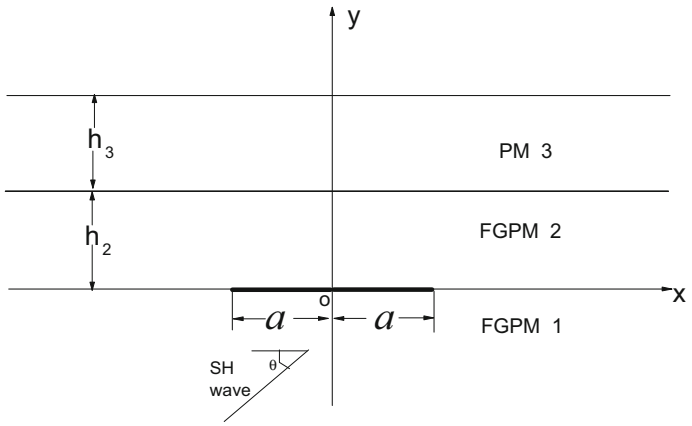

Fig. 1 Scattering of the SH wave by a limited permeable in a FGPM bonded to a PM

in-plane electric field are coupled. The constitutive equation can be written as:

$$\tau_{yzk} = c_{44k}(y)\frac{\partial w_k}{\partial y} + e_{15k}(y)\frac{\partial \varphi_k}{\partial y}, \qquad \tau_{xzk} = c_{44k}(y)\frac{\partial w_k}{\partial x} + e_{15k}(y)\frac{\partial \varphi_k}{\partial x}, \tag{1}$$

$$D_{yk} = e_{15k}(y)\frac{\partial w_k}{\partial y} - \varepsilon_{11(k)}(y)\frac{\partial \varphi_k}{\partial y}, \qquad D_{xk} = e_{15k}(y)\frac{\partial w_k}{\partial x} - \varepsilon_{11k}(y)\frac{\partial \varphi_k}{\partial x} \tag{2}$$

where τ_{lzk}, w_k, D_{lk}, and $\varphi_k (l = x, y, k = 1, 2, 3)$ are the shear stresses, anti-plane displacements, in-plane electric displacements, and electric potentials, respectively. The variations in material constants $c_{44k}(y)$, $e_{15k}(y)$, and $\varepsilon_{11k}(y)$ called the shear modulus, the piezoelectric coefficients, the dielectric parameter, respectively, are assumed in the following exponential forms:

$$\begin{aligned} &c_{44k}(y) = c_{440}e^{2\beta y},\ e_{15k}(y) = e_{150}e^{2\beta y},\ \varepsilon_{11k}(y) = \varepsilon_{110}e^{2\beta y},\ \rho_k(y) = \rho_0 e^{2\beta y}, \\ &c_{443}(y) = c_{440}e^{2\beta h_2},\ e_{153}(y) = e_{150}e^{2\beta h_2},\ \varepsilon_{113}(y) = \varepsilon_{110}e^{2\beta h_2},\ \rho_3(y) = \rho_0 e^{2\beta h_2} \end{aligned} \tag{3}$$

where β is the material gradient and ρ is the mass density. c_{440}, e_{150}, ε_{110}, and ρ_0 are shear modulus, piezoelectric constant, dielectric coefficient, and mass density at $y = 0$, respectively.

The electric fields E_{xk} and E_{yk} are related to the electric potential φ_k by the following form:

$$E_{xk} = -\frac{\partial \varphi_k}{\partial x}, \qquad E_{yk} = -\frac{\partial \varphi_k}{\partial y}. \tag{4}$$

Let a time-harmonic SH wave originating at $y \to \infty$ be incident with an incidence angle θ on the crack. The anti-plane shear stress acts on the materials, so the displacement components are written as:

$$w^{(t)}(x, y, t) = w^{(i)}(x, y, t) + w(x, y, t) \tag{5}$$

where $w^{(t)}(x, y, t)$, $w^{(i)}(x, y, t)$, and $w(x, y, t)$ are the total field, incidence field, and scattering field. The appended superscripts "t" and "i" mean "total" and "incident," respectively. In the incidence field, the displacement and the electric potential are expressed as [27]

$$w^{(i)}(x, y, t) = A_0 \exp\left[-i\omega\left(\frac{x\cos\theta + y\sin\theta}{c_{\text{sh}}} + t\right)\right], \tag{6}$$

$$\varphi^{(i)}(x, y, t) = \frac{e_{15}}{\varepsilon_{11}} A_0 \exp\left[-i\omega\left(\frac{xcos\theta + ysin\theta}{c_{\text{sh}}} + t\right)\right] \tag{7}$$

where A_0, θ, ω, and t are the amplitude, the incidence angle, the frequency and time, c_{sh} is the shear wave velocity. $i = \sqrt{-1}$, $c_{\text{sh}} = \sqrt{\frac{\mu_0}{\rho_0}}$, $\mu_0 = c_{440} + \frac{e_{150}^2}{\varepsilon_{110}}$.

Because of the same time factor in the incidence and the scattering fields, the displacement and electric potential in the scattering field are expressed as follows:

$$w_k(x, y, t) = w(x, y)\exp(-i\omega t), \qquad \varphi_k(x, y, t) = \varphi(x, y)\exp(-i\omega t). \tag{8}$$

In view of the harmonic time variation in the incident wave given by Eqs. (6) and (7), the field quantities will all contain the time factor $\exp(-i\omega t)$, which will henceforth be dropped.

Substituting Eqs. (6–7) into Eqs. (1–2) and applying Eq. (3), the stress in the incidence field will be written as:

$$\tau_0 = \tau_{yz}^{(i)}(x, 0, t) = \tau_{00}\sin\theta\exp\left(-i\omega\frac{x\cos\theta}{c_{\mathrm{sh}}}\right) \tag{9}$$

where

$$\tau_{00} = -iA_0\omega\rho_0 c_{\mathrm{sh}}. \tag{10}$$

The equilibrium equations of the PM can be expressed as follows:

$$\frac{\partial\tau_{xzk}}{\partial x} + \frac{\partial\tau_{yzk}}{\partial y} = \rho\frac{\partial^2 w_k}{\partial t^2}, \qquad \frac{\partial D_{xk}}{\partial x} + \frac{\partial D_{yk}}{\partial y} = 0. \tag{11}$$

Substituting Eqs. (1–2) and (8) into Eq. (11) and using the relation (3), we obtain the following equations:

$$\nabla^2 w_k + 2\beta\frac{\partial w_k}{\partial y} + \frac{\rho_0\omega^2}{\mu_0}w_k = 0, \tag{12}$$

$$\nabla^2\phi_k + 2\beta\frac{\partial\phi_k}{\partial y} = 0, \tag{13}$$

$$\nabla^2 w_3 + \frac{\rho_0\omega^2}{\mu_0}w_3 = 0, \tag{14}$$

$$\nabla^2\phi_3 = 0 \tag{15}$$

where the Bleustein function is given by $\phi_k = \varphi_k - \frac{e_{150}}{\varepsilon_{110}}w_k$, and $\nabla^2 = \frac{\partial^2}{\partial x^2} + \frac{\partial^2}{\partial y^2}$ is the two-dimensional Laplace operator.

On the surfaces $y = h_2+h_3$, $y = h_2$ and $y = 0$, the traction and electric displacement boundary conditions are

$$\tau_{yz3}(x, h_2 + h_3) = 0, \qquad D_{y3}(x, h_2 + h_3) = 0, \tag{16}$$

$$\tau_{yz2}(x, h_2) = \tau_{yz3}(x, h_2), \quad w_2(x, h_2) = w_3(x, h_2), \tag{17}$$

$$D_{y2}(x, h_2) = D_{y3}(x, h_2), \quad \varphi_2(x, h_2) = \varphi_3(x, h_2), \tag{18}$$

$$\tau_{yz1}(x, 0) = \tau_{yz2}(x, 0), \quad D_{y1}(x, 0) = D_{y2}(x, 0), \quad (a \le x < \infty). \tag{19}$$

The mechanical boundary conditions at the surfaces of the cracks are assumed to be traction-free. Following Refs. [24,25], the limited permeable crack boundary condition on the cracked plane $y = 0$ in scattering field is written as:

$$\tau_{yz1}(x, 0) = \tau_{yz2}(x, 0) = -\tau_{yz}^{(i)}(x, 0, t) = -\tau_0, \quad (0 \le x < a), \tag{20}$$

$$w_1(x, 0) = w_2(x, 0), \quad (a \le x < \infty), \tag{21}$$

$$D_{y1}(x, 0) = D_{y2}(x, 0) = D_y^c - D_0 = G_0, \quad (0 \le x < a), \tag{22}$$

$$\varphi_1(x, 0) = \varphi_2(x, 0), \quad (a \le x < \infty) \tag{23}$$

where the quantities τ_0 and D_0 are, respectively, the stress and electric displacement in the absence of any cracks. Equations (22) and (23) will be hereafter referred to the "limited" crack boundary condition. And D_y^c is the normal component of the electric displacement on the crack faces.

3 Dual integral equations

Applying first Fourier transforms to the governing equations of Eqs. (12–15) and then taking inverse Fourier transforms, the following results are obtained:

$$w_1(x,y)=\frac{1}{2\pi}\int_{-\infty}^{\infty}A_1(s)e^{\lambda_1 y}e^{-isx}\mathrm{d}s, \tag{24}$$

$$\varphi_1(x,y)=\frac{e_{150}}{\varepsilon_{110}}w_1(x,y)+\frac{1}{2\pi}\int_{-\infty}^{\infty}B_1(s)e^{\gamma_1 y}e^{-isx}\mathrm{d}s, \tag{25}$$

$$w_2(x,y)=\frac{1}{2\pi}\int_{-\infty}^{\infty}\left[A_2(s)e^{\lambda_1 y}+A_3(s)e^{\lambda_2 y}\right]e^{-isx}\mathrm{d}s, \tag{26}$$

$$\varphi_2(x,y)=\frac{e_{150}}{\varepsilon_{110}}w_2(x,y)+\frac{1}{2\pi}\int_{-\infty}^{\infty}\left[B_2(s)e^{\gamma_1 y}+B_3(s)e^{\gamma_2 y}\right]e^{-isx}\mathrm{d}s, \tag{27}$$

$$w_3(x,y)=\frac{1}{2\pi}\int_{-\infty}^{\infty}\left[C_1(s)e^{my}+C_2(s)e^{-my}\right]e^{-isx}\mathrm{d}s, \tag{28}$$

$$\varphi_3(x,y)=\frac{e_{150}}{\varepsilon_{110}}w_3(x,y)+\frac{1}{2\pi}\int_{-\infty}^{\infty}\left[D_1(s)e^{sy}+D_2(s)e^{-sy}\right]e^{-isx}\mathrm{d}s \tag{29}$$

where

$$\lambda_1=-\beta+\sqrt{\beta^2+s^2-\frac{\rho_0\omega^2}{\mu_0}},\quad \lambda_2=-\beta-\sqrt{\beta^2+s^2-\frac{\rho_0\omega^2}{\mu_0}},\quad \gamma_1=-\beta+\sqrt{\beta^2+s^2},$$

$$\gamma_2=-\beta-\sqrt{\beta^2+s^2},\quad m=\sqrt{s^2-\frac{\rho_0\omega^2}{\mu_0}}.$$

The solutions of the undetermined functions $A_l(s)$, $B_l(s)$, $C_j(s)$, and $D_j(s)(l=1,2,3,\ j=1,2)$ depend on the mechanical and electric conditions of the crack surfaces.

From Eqs. (24–29), (1), and (2), the stress and the electric displacement can be obtained,

$$\tau_{yz1}(x,y)=\frac{\mu_0 e^{2\beta y}}{2\pi}\int_{-\infty}^{\infty}\lambda_1 A_1(s)e^{\lambda_1 y}e^{-isx}\mathrm{d}s+\frac{e_{150}e^{2\beta y}}{2\pi}\int_{-\infty}^{\infty}\gamma_1 B_1(s)e^{\gamma_1 y}e^{-isx}\mathrm{d}s, \tag{30}$$

$$D_{y1}(x,y)=-\frac{\varepsilon_{110}e^{2\beta y}}{2\pi}\int_{-\infty}^{\infty}\gamma_1 B_1(s)e^{\gamma_1 y}e^{-isx}\mathrm{d}s, \tag{31}$$

$$\begin{aligned}\tau_{yz2}(x,y)=&\frac{\mu_0 e^{2\beta y}}{2\pi}\int_{-\infty}^{\infty}\left[\lambda_1 A_2(s)e^{\lambda_1 y}+\lambda_2 A_3(s)e^{\lambda_2 y}\right]e^{-isx}\mathrm{d}s\\&+\frac{e_{150}e^{2\beta y}}{2\pi}\int_{-\infty}^{\infty}[\gamma_1 B_2(s)e^{\gamma_1 y}+\gamma_2 B_3(s)e^{\gamma_2 y}]e^{-isx}\mathrm{d}s,\end{aligned} \tag{32}$$

$$D_{y2}(x,y)=-\frac{\varepsilon_{110}e^{2\beta y}}{2\pi}\int_{-\infty}^{\infty}\left[\gamma_1 B_2(s)e^{\gamma_1 y}+\gamma_2 B_3(s)e^{\gamma_2 y}\right]e^{-isx}\mathrm{d}s, \tag{33}$$

$$\begin{aligned}\tau_{yz3}(x,y)=&\frac{\mu_0 e^{2\beta h_2}}{2\pi}\int_{-\infty}^{\infty}m\left[C_1(s)e^{my}-C_2(s)e^{-my}\right]e^{-isx}\mathrm{d}s\\&+\frac{e_{150}e^{2\beta h_2}}{2\pi}\int_{-\infty}^{\infty}s\left[D_1(s)e^{sy}-D_2(s)e^{-sy}\right]e^{-isx}\mathrm{d}s,\end{aligned} \tag{34}$$

$$D_{y3}(x,y)=-\frac{\varepsilon_{110}e^{2\beta h_2}}{2\pi}\int_{-\infty}^{\infty}s\left[D_1(s)e^{sy}-D_2(s)e^{-sy}\right]e^{-isx}\mathrm{d}s. \tag{35}$$

Using boundary conditions (19), from the second of Eqs. (30)–(33), we have

$$\lambda_1[A_1(s)-A_2(s)]=\lambda_2 A_3(s)\triangleq M(s), \tag{36}$$

$$\gamma_1[B_1(s)-B_2(s)]=\gamma_2 B_3(s)\triangleq N(s) \tag{37}$$

where $M(s)$ and $N(s)$ are to be determined.

Substituting the solutions of 10 unknown functions $A_1(s)$, $A_2(s)$, $A_3(s)$, $B_1(s)$, $B_2(s)$, $B_3(s)$, $C_1(s)$, $C_2(s)$, $D_1(s)$, $D_2(s)$ (the solutions can be found in "Appendix B") into Eqs. (24–25) and (30–31), and applying the boundary conditions (20–23), two simultaneous dual integral equations can be obtained as follows:

$$\frac{1}{2\pi}\int_{-\infty}^{\infty} sF_1(s)P_1(s)e^{-isx}\mathrm{d}s = \frac{1}{\mu_0}[\tau_{00}\sin\theta\exp\left(-i\omega\frac{x\cos\theta}{c_{\mathrm{sh}}}\right) - \frac{e_{150}}{\varepsilon_{110}}G_0] \quad (0 \le x < a), \tag{38}$$

$$\frac{1}{2\pi}\int_{-\infty}^{\infty} P_1(s)e^{-isx}\mathrm{d}s = 0 \quad (x \ge a), \tag{39}$$

$$\frac{1}{2\pi}\int_{-\infty}^{\infty} sF_2(s)P_2(s)e^{-isx}\mathrm{d}s = \frac{G_0}{\varepsilon_{110}} \quad (0 \le x < a), \tag{40}$$

$$\frac{1}{2\pi}\int_{-\infty}^{\infty} \left[\frac{e_{150}}{\varepsilon_{110}}P_1(s) + P_2(s)\right]e^{-isx}\mathrm{d}s = 0 \quad (x \ge a) \tag{41}$$

where $F_1(s)$, $F_2(s)$ are known functions (see "Appendix C"), and

$$P_1(s) = \frac{1}{2}\frac{\lambda_2 - \lambda_1}{\lambda_2\lambda_1}M(s), \quad P_2(s) = \frac{1}{2}\frac{\gamma_2 - \gamma_1}{\gamma_2\gamma_1}N(s).$$

Solving the dual integral Eqs. (38–41) by using the Copson–Sih method [26], the solutions can be expressed as

$$P_1(s) = \frac{a^2}{\mu_0}\left(\tau_{00}\sin\theta - \frac{e_{150}}{\varepsilon_{110}}G_0\right)\int_0^1 \sqrt{\xi}\,[\Omega_1(\xi)J_0(sa\xi) + \Omega_2(\xi)J_1(sa\xi)]\,\mathrm{d}\xi, \tag{42}$$

$$P_2(s) = \frac{a^2G_0}{\varepsilon_{110}}\int_0^1 \sqrt{\xi}\,[\Omega_3(\xi)J_0(sa\xi) + \Omega_4(\xi)J_1(sa\xi)]\,\mathrm{d}\xi \tag{43}$$

where $J_0(sa\xi)$ and $J_1(sa\xi)$ are the zero-order Bessel function and the first-order Bessel function of the first kind. The functions $\Omega_1(\xi)$, $\Omega_2(\xi)$, $\Omega_3(\xi)$, and $\Omega_4(\xi)$ can be governed by the Fredholm integral equation of the second kind,

$$\begin{aligned}
\Omega_1(\xi) + \int_0^1 \Omega_1(\eta)K_1(\xi,\eta)\mathrm{d}\eta &= \sqrt{\xi}J_0\left(\frac{\omega}{c_{\mathrm{sh}}}a\xi\cos\theta\right),\\
\Omega_2(\xi) + \int_0^1 \Omega_2(\eta)K_2(\xi,\eta)\mathrm{d}\eta &= \sqrt{\xi}J_1\left(\frac{\omega}{c_{\mathrm{sh}}}a\xi\cos\theta\right),
\end{aligned} \tag{44}$$

$$\begin{aligned}
\Omega_3(\xi) + \int_0^1 \Omega_3(\eta)K_3(\xi,\eta)\mathrm{d}\eta &= \sqrt{\xi}J_0\left(\frac{\omega}{c_{\mathrm{sh}}}a\xi\cos\theta\right),\\
\Omega_4(\xi) + \int_0^1 \Omega_4(\eta)K_4(\xi,\eta)\mathrm{d}\eta &= \sqrt{\xi}J_1\left(\frac{\omega}{c_{\mathrm{sh}}}a\xi\cos\theta\right),
\end{aligned} \tag{45}$$

with kernel functions $K_1(\xi,\eta)$, $K_2(\xi,\eta)$, $K_3(\xi,\eta)$ and $K_4(\xi,\eta)$ given by

$$\begin{aligned}
K_1(\xi,\eta) &= \sqrt{\xi\eta}\int_0^\infty s\left[F_1\left(\frac{s}{a}\right) - 1\right]J_0(s\xi)J_0(s\eta)\mathrm{d}s,\\
K_2(\xi,\eta) &= \sqrt{\xi\eta}\int_0^\infty s\left[F_1\left(\frac{s}{a}\right) - 1\right]J_1(s\xi)J_1(s\eta)\mathrm{d}s,
\end{aligned} \tag{46}$$

$$\begin{aligned}
K_3(\xi,\eta) &= \sqrt{\xi\eta}\int_0^\infty s\left[F_2\left(\frac{s}{a}\right) - 1\right]J_0(s\xi)J_0(s\eta)\mathrm{d}s,\\
K_4(\xi,\eta) &= \sqrt{\xi\eta}\int_0^\infty s\left[F_2\left(\frac{s}{a}\right) - 1\right]J_1(s\xi)J_1(s\eta)\mathrm{d}s.
\end{aligned} \tag{47}$$

4 The stress intensity factor

By using the formula of integration by parts, Eqs. (42) and (43) can be written as:

$$P_1(s) = \frac{\tau_{00} a}{\mu_0} (\sin\theta + \wedge_0) \frac{1}{s} [\Omega_1(1) J_1(sa) + \Omega_2(1) J_2(sa) + \cdots], \tag{48}$$

$$P_2(s) = \frac{a D_0 (D_r - 1)}{\varepsilon_{110}} \frac{1}{s} [\Omega_1(1) J_1(sa) + \Omega_2(1) J_2(sa) + \cdots] \tag{49}$$

where $\wedge_0 = \lambda_0(1 - D_r)$, $\lambda_0 = \frac{e_{150}}{\varepsilon_{110}} \frac{D_0}{\tau_{00}}$ is electric load, $D_r = \frac{D_y^c}{D_0}$ is electric boundary condition, and $J_2(sa)$ denotes for the second-order Bessel function of the first kind.

Substituting Eqs. (48–49) into Eqs. (30–31), part of the stress and the electric displacement stresses can be obtained,

$$\begin{aligned} \tau_{yz1}(x, 0) = &-a\tau_{00}(\sin\theta + \wedge_0) \int_{-\infty}^{\infty} F_1(s) [\Omega_1(1) J_1(sa) + \Omega_2(1) J_2(sa)] e^{-isx} \mathrm{d}s \\ &+ a\tau_{00} \wedge_0 \int_{-\infty}^{\infty} F_2(s) [\Omega_3(1) J_1(sa) + \Omega_4(1) J_2(sa)] e^{-isx} \mathrm{d}s, \end{aligned} \tag{50}$$

$$D_{y1}(x, 0) = a D_0 (D_r - 1) \int_{-\infty}^{\infty} F_2(s) [\Omega_3(1) J_1(sa) + \Omega_4(1) J_2(sa)] e^{-isx} \mathrm{d}s. \tag{51}$$

Considering the stress singularity as $s \to \infty$, the result is

$$F_1(s) \to 1, \quad F_2(s) \to 1,$$

introducing the complex transformations as follows:

$$z = x + iy = r \exp(i\theta), \quad z - a = r_1 \exp(i\theta_1), \quad z + a = r_2 \exp(i\theta_2).$$

Thus, Eqs. (50–51) can be written as:

$$\tau_{yz1}(x, 0) = \tau_{00} \{(\sin\theta + \wedge_0) [\Omega_1(1) - \mathrm{i}\Omega_2(1)] - \wedge_0 [\Omega_3(1) - \mathrm{i}\Omega_4(1)]\} \frac{x}{\sqrt{(x + a)(x - a)}}, \tag{52}$$

$$D_{y1}(x, 0) = D_0(1 - D_r) [\Omega_3(1) - \mathrm{i}\Omega_4(1)] \frac{x}{\sqrt{(x + a)(x - a)}}. \tag{53}$$

According to Eqs. (52–53), the mode-III dynamic stress intensity factor and the electric displacement intensity factor for the limited permeable case are obtained as follows:

$$\begin{aligned} K^T &= \lim_{x \to a^+} \sqrt{2\pi(x - a)} \tau_{yz1}(x, 0) \\ &= \sqrt{\pi a} \tau_{00} \{(\sin\theta + \wedge_0) [\Omega_1(1) - \mathrm{i}\Omega_2(1)] - \wedge_0 [\Omega_3(1) - \mathrm{i}\Omega_4(1)]\}, \end{aligned} \tag{54}$$

$$K^D = \lim_{x \to a^+} \sqrt{2\pi(x - a)} D_{y1}(x, 0) = \frac{\varepsilon_{110}}{e_{150}} \wedge_0 \sqrt{\pi a} \tau_{00} [\Omega_3(1) - \mathrm{i}\Omega_4(1)]. \tag{55}$$

Then, the NDSIF is obtained as follows:

$$K_3 = |(\sin\theta + \wedge_0) [\Omega_1(1) - \mathrm{i}\Omega_2(1)] - \wedge_0 [\Omega_3(1) - \mathrm{i}\Omega_4(1)]|.$$

5 Numerical computation and discussion

By using the numerical integral method, the numerical solution of $\Omega_1(1)$ and $\Omega_2(1)$ can be determined from Eqs. (44) and (46), and the numerical solution of $\Omega_3(1)$ and $\Omega_4(1)$ can be obtained from Eqs. (45) and (47). In this section, we will investigate the effect of the gradient parameter, the electric loads, electric boundary condition, the incident angle, thickness of PM strip, the distance from the crack to the interface, and wave number on the NDSIF. The numerical results are shown in Figs. 2, 3, 4, 5, 6, 7, and 8.

The variations in the NDSIF K_3 versus wave number $a\omega/c_{\mathrm{sh}}$ for different incident angles θ are shown in Fig. 2. It is indicated by Fig. 2 that the NDSIF increases remarkably with increasing θ. So, a larger angle of

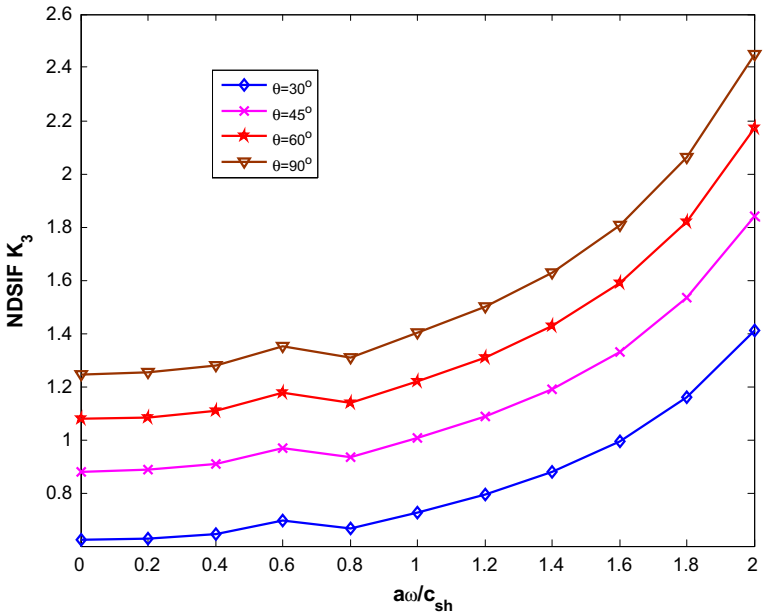

Fig. 2 Variations in the NDSIF K_3 with $a\omega/c_{\mathrm{sh}}$ for different θ (limited permeable crack $\beta a = 0.5$, $D_r = 0.3$, $\lambda_0 = 0.6$, $h_2/a = 0.4$, $h_3/a = 0.5$)

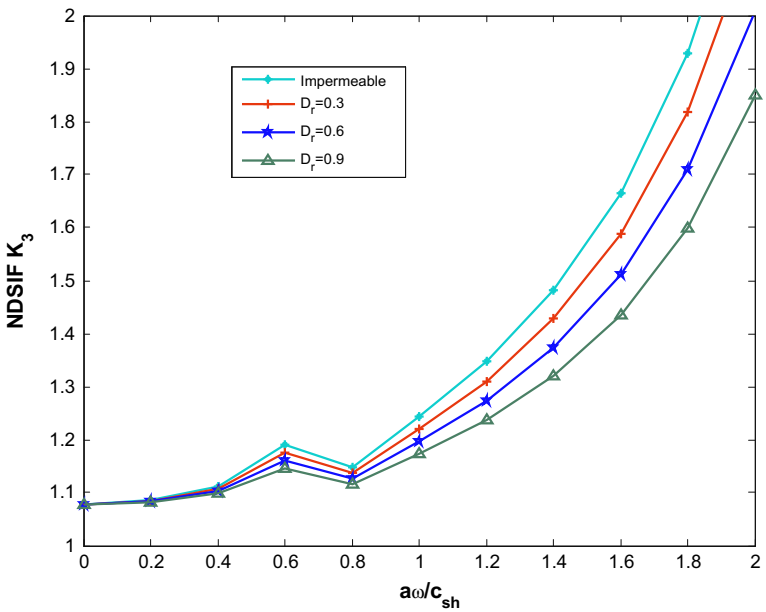

Fig. 3 Variations in the NDSIF K_3 with $a\omega/c_{\mathrm{sh}}$ for different D_r (impermeable and limited permeable crack)

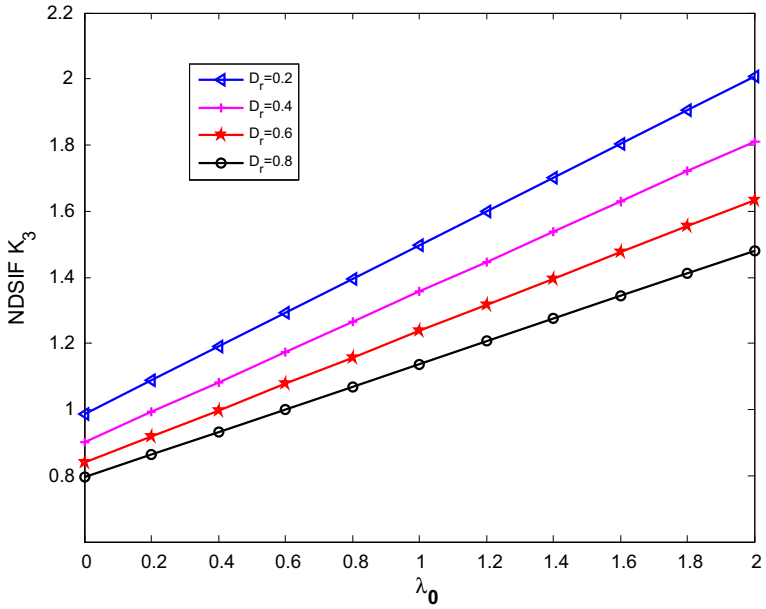

Fig. 4 Variations in the NDSIF K_3 with λ_0 for different D_r (limited permeable crack)

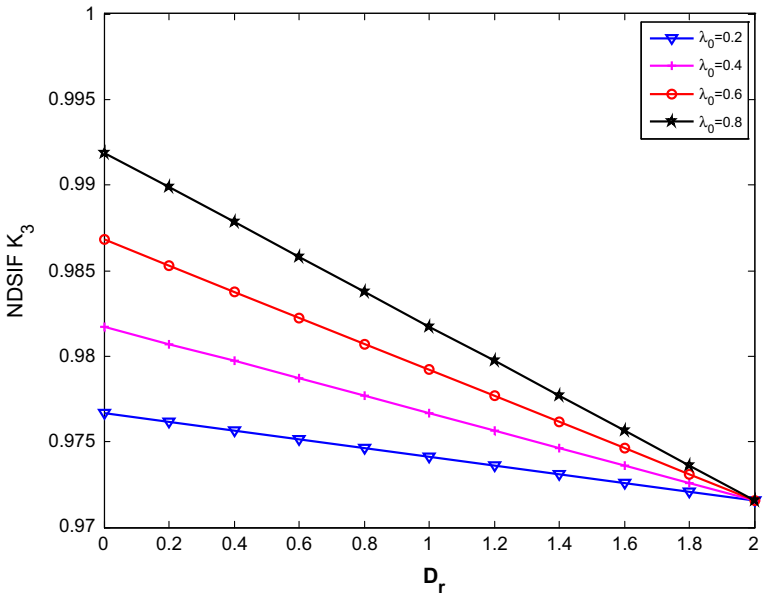

Fig. 5 Variations in the NDSIF K_3 with D_r for different λ_0 (limited permeable crack)

incidence can inhibit the peak emergence of the NDSIF, which means that the incidence angle can control the NDSIF of the material. Therefore, it can inhibit material properties and crack propagation by adjusting properly the load angle of incidence.

For an impermeable and limited permeable crack, Fig. 3 displays the effect of the electric boundary condition D_r on the NDSIF K_3, where $\beta a = 0.5, \lambda_0 = 0.6, \theta = \pi/3, h_2/a = 0.4$, and $h_3/a = 0.5$. Figure 4 demonstrates the effect of electric loads λ_0 on the normalized dynamic stress intensity factor (NDSIF) K_3 under different D_r, where $a\omega/c_{\text{sh}} = 0.2$, $\beta a = 0.5$, $\theta = \pi/3, h_2/a = 0.4, h_3/a = 0.5$. The effect of the electric boundary condition D_r on the NDSIF K_3 under different λ_0 is illustrated in Fig. 5, where $\beta a = 1.0, a\omega/c_{\text{sh}} = 0.2, \theta = \pi/3, h_2/a = 0.4$, and $h_3/a = 0.5$. Looking at Figs. 3, 4, and 5, it is found that the NDSIF generally decreases with increasing D_r, which delineates that being in a more permeable state,

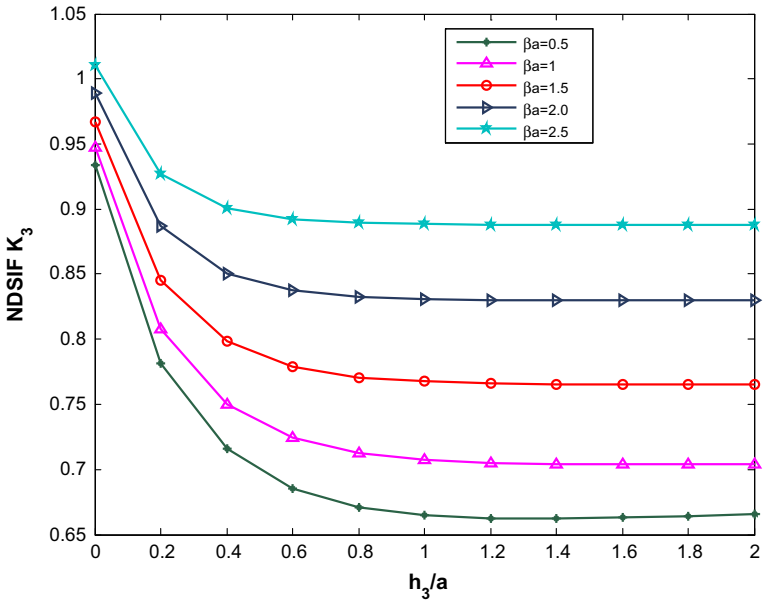

Fig. 6 Variations in the NDSIF K_3 with h_3/a for different βa (limited permeable crack $a\omega/c_{\mathrm{sh}} = 0.5, \theta = \pi/6, h_2/a = 0.4, D_r = 0.5, \lambda_0 = 2.0$)

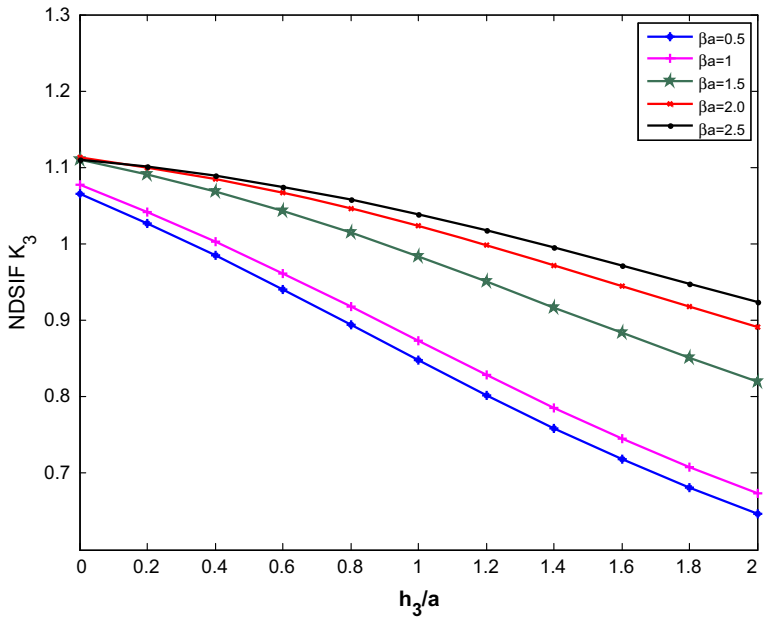

Fig. 7 Variations in the NDSIF K_3 with h_3/a for different βa (permeable crack $a\omega/c_{\mathrm{sh}} = 0.5, \theta = \pi/6, h_2/a = 0.4, \lambda_0 = 2.0$)

the crack propagation may be resisted. From Figs. 4 and 5, the NDSIF increases with increasing λ_0, which illustrates that a smaller electric load may lead to a smaller potential of the crack propagation.

In addition, from Figs. 2 and 3, the NDSIF tends to increase with an increase in the wave number $a\omega/c_{\mathrm{sh}}$. So, in engineering, it can decrease the crack tip extension by adjusting the frequency of the SH wave. At the same time, it can realize the change in the stress field by changing the frequency of the incident wave.

Figures 6 and 7 indicate the influence of the thickness of the PM layer h_3/a on the NDSIF K_3 under different gradient parameters βa. It can also be found from Figs. 6 and 7 that the NDSIF decreases with the

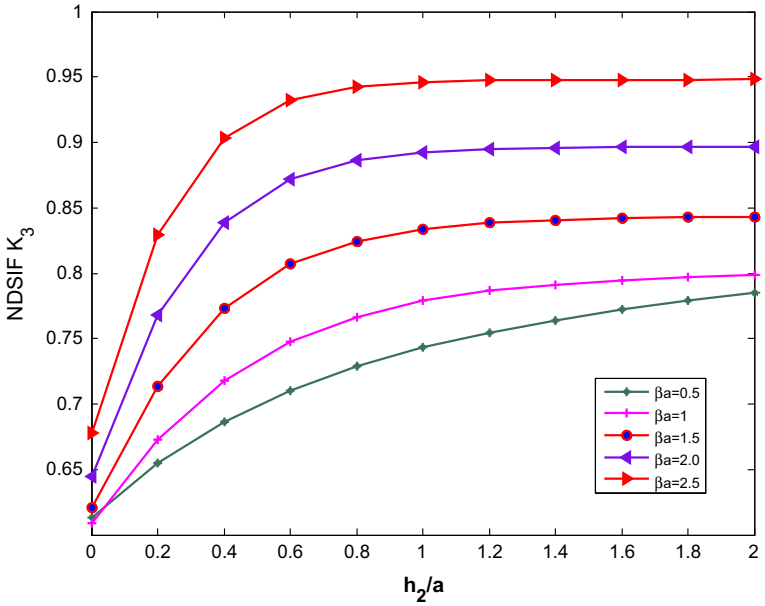

Fig. 8 Variations in the NDSIF K_3 with h_2/a for different βa (limited permeable crack)

increase of h_3/a when βa is fixed. So, we could conclude that the propagation of the crack can be resisted by properly increasing the thickness of the PM.

Under different gradient parameters βa, the effect of the distance from the crack to the interface h_2/a on the NDSIF K_3 is illustrated in Fig. 8, where $a\omega/c_{\text{sh}} = 0.5, \theta = \pi/6, h_3/a = 0.5 D_r = 0.5, \lambda_0 = 0.2$. It is found in Fig. 8 that the NDSIF increases with the decrease in h_2/a when βa is fixed. So, in practical engineering, it can improve the fracture resistance of materials by controlling properly the distance from the crack to the interface.

From Figs. 6, 7, and 8, the NDSIF tends to increase with an increase in the gradient parameter βa, which indicates that the stress concentration around the crack tips may be relieved by adjusting the graded parameters.

6 Conclusions

Scattering of an SH wave by a limited permeable crack in a functionally graded piezoelectric substrate bonded to a homogeneous piezoelectric strip has been solved by means of the Fourier transform–Copson method. The crack is considered as mechanically free and electrically limited permeable. Also, the field intensity factors have been obtained via auxiliary functions determined from Fredholm integral equations. The dynamic stress intensity factor depends on the gradient parameter, the electric loads, electric boundary conditions, the angle of wave, thickness of PM strip, the distance from the crack to the interface, and wave number. Unlike the traditional impermeable and permeable crack assumptions, the present limited permeable crack boundary condition is considered to be neither electrically insulating nor electrically conducting. In real piezoelectric ceramics, the solutions derived from the limbed permeable boundary condition provide more reasonable results, which are located between those obtained from an impermeable crack and permeable crack analysis.

7 Case studies

The solutions provided in the previous sections can now be extended to several special cases, as detailed below.

Case 1 Static solution. The corresponding static solution is obtained by letting $\frac{\rho_0 \omega^2}{\mu_0} = 0$. For this case, all the auxiliary functions Ω_1, Ω_2, Ω_3 and Ω_4 are governed by

$$\lambda_1 = \gamma_1 = -\beta + \sqrt{\beta^2 + s^2}, \quad \lambda_2 = \gamma_2 = -\beta - \sqrt{\beta^2 + s^2}, m = s,$$
$$F_1(s) = F_2(s) = \frac{2\lambda_1\lambda_2}{s(\lambda_2 - \lambda_1)} Q(s), \quad R(s) = Q(s).$$

Case 2 Homogeneous solution. To find the solutions for the homogeneous piezoelectric materials, one should let $\beta = 0$. In this case,

$$p_1 = \sqrt{s^2 - \frac{\rho_0\omega^2}{\mu_0}}, \quad p_2 = -\sqrt{s^2 - \frac{\rho_0\omega^2}{\mu_0}}, \quad q_1 = s, \quad q_2 = -s,$$
$$H_1(s) = \frac{1 - e^{2sh_3}}{1 + e^{2sh_3}}, \quad H_2(s) = \frac{1 - e^{2mh_3}}{1 + e^{2mh_3}}.$$

Case 3 Interface crack. For the case of $h_2 = 0$,

$$Q(s) = 1 - \frac{\lambda_1}{\lambda_2}\frac{\lambda_2 - sH_1(s)}{\lambda_1 - sH_1(s)}, \quad R(s) = 1 - \frac{\gamma_1}{\gamma_2}\frac{\gamma_2 - mH_2(s)}{\gamma_1 - mH_2(s)}.$$

Case 4 Considering $h_3 \to 0$, we can find the solution of a semi-infinite FGPM in the form

$$H_1(s) = H_2(s) = 0, \quad Q(s) = 1 - e^{(\lambda_2 - \lambda_1)h_2}, \quad R(s) = 1 - e^{(\gamma_2 - \gamma_1)h_2}.$$

Acknowledgments This work was supported by the National Natural Science Foundation of China (11362018) and the Research Fund for the Doctoral Program of Higher Education of China (20116401110002)

Appendix A

To obtain the conventional solutions based on the impermeable and the permeable crack assumptions, we must find the value of an unknown constant D_y^c (or D_r) which is contained in Eqs. (54) and (55). Firstly, by letting $D_r = 0$ (or $\wedge_0 = \lambda_0$), the impermeable solutions are easily obtained as:

$$K^T = \sqrt{\pi a}\tau_{00}\left\{(\sin\theta + \lambda_0)\left[\Omega_1(1) - \mathrm{i}\Omega_2(1)\right] - \lambda_0\left[\Omega_3(1) - \mathrm{i}\Omega_4(1)\right]\right\}, \tag{A.1}$$
$$K^D = \frac{\varepsilon_{110}}{e_{150}}\lambda_0\sqrt{\pi a}\tau_{00}\left[\Omega_3(1) - \mathrm{i}\Omega_4(1)\right]. \tag{A.2}$$

In order to obtain the permeable solution, one replaces Eq. (22) with the following:

$$D_{y1}(x, 0) = D_{y2}(x, 0), \quad \varphi_1(x, 0) = \varphi_2(x, 0), \quad (0 \le x < a) \tag{A.3}$$

or

$$D_{y1}(x, 0) = D_{y2}(x, 0), \quad E_{x1}(x, 0) = E_{x2}(x, 0), \quad (0 \le x < a). \tag{A.4}$$

Following the same procedure as shown in Sect. 3, it leads to two pairs of dual integral equations from Eqs. (20), (21), (A.4), and (23),

$$\frac{1}{2\pi}\int_{-\infty}^{\infty} sF(s)p(s)\cos(sx)\mathrm{d}s = \frac{\tau_{00}}{c_{440}}\sin\theta\exp\left(-i\omega\frac{x\cos\theta}{c_{\mathrm{sh}}}\right), \quad (0 \le x < a), \tag{A.5}$$
$$\frac{1}{2\pi}\int_{-\infty}^{\infty} p(s)\cos(sx)\mathrm{d}s = 0 \quad (x > a), \tag{A.6}$$
$$\frac{1}{2\pi}\int_{-\infty}^{\infty} s\left[\left(\frac{q_2 - q_1}{q_2q_1}\right)N(s) + \frac{e_{150}}{\varepsilon_{110}}\left(\frac{p_2 - p_1}{p_2p_1}\right)M(s)\right]\sin(sx)\mathrm{d}s = 0, \quad (0 \le x < a), \tag{A.7}$$
$$\frac{1}{2\pi}\int_{-\infty}^{\infty} \left[\left(\frac{q_2 - q_1}{q_2q_1}\right)N(s) + \frac{e_{150}}{\varepsilon_{110}}\left(\frac{p_2 - p_1}{p_2p_1}\right)M(s)\right]\cos(sx)\mathrm{d}s = 0, \quad (x > a) \tag{A.8}$$

where

$$F(s)=\frac{s^2-\frac{\rho_0\omega^2}{\mu_0}}{s\sqrt{\beta^2+s^2-\frac{\rho_0\omega^2}{\mu_0}}}f(s),\quad f(s)=\left(1+\kappa_0^2\right)Q(s)-\kappa_0^2R(s),\quad \kappa_0=\sqrt{\frac{e_{150}^2}{c_{440}\varepsilon_{110}}}.$$

It is readily seen from Eqs. (A.7) and (A.8) that

$$N(s)=-\frac{e_{150}}{\varepsilon_{110}}\frac{M(s)}{J(s)}$$

where $J(s)=\frac{q_2-q_1}{q_2q_1}\frac{p_2p_1}{p_2-p_1}$.

With the aid of Copson's method [26] in the above Eqs. (A.5) and (A.6), one finally obtains a Fredholm integral equation of the second kind of the form:

$$\begin{aligned}\Psi_1(\xi)+\int_0^1\Psi_1(\eta)K_1(\xi,\eta)\mathrm{d}\eta&=\sqrt{\xi}J_0\left(\frac{w}{c_{\mathrm{sh}}}a\xi\cos\theta\right),\\ \Psi_2(\xi)+\int_0^1\Psi_2(\eta)K_2(\xi,\eta)\mathrm{d}\eta&=\sqrt{\xi}J_1\left(\frac{w}{c_{\mathrm{sh}}}a\xi\cos\theta\right)\end{aligned}\tag{A.9}$$

where

$$\begin{aligned}K_1(\xi,\eta)&=\sqrt{\xi\eta}\int_0^\infty s\left[F\left(\frac{s}{a}\right)-1\right]J_0(s\xi)J_0(s\eta)\mathrm{d}s,\\ K_2(\xi,\eta)&=\sqrt{\xi\eta}\int_0^\infty s\left[F\left(\frac{s}{a}\right)-1\right]J_1(s\xi)J_1(s\eta)\mathrm{d}s.\end{aligned}\tag{A.10}$$

Two field intensity factors are given as:

$$\begin{aligned}K^T&=\lim_{x\to a^+}\sqrt{2\pi(x-a)}\tau_{yz1}(x,0)=\sqrt{\pi a}\tau_{00}\left[\Psi_1(1)-\mathrm{i}\Psi_2(1)\right]\sin\theta,\\ K^D&=\lim_{x\to a^+}\sqrt{2\pi(x-a)}D_{y1}(x,0)=\frac{e_{150}}{c_{440}}\sqrt{\pi a}\tau_{00}[\Psi_1(1)-\mathrm{i}\Psi_2(1)]\sin\theta=\frac{e_{150}}{c_{440}}K^T.\end{aligned}\tag{A.11}$$

Appendix B

Substituting Eqs. (26–29) and (32–35) into Eqs. (16–18), and applying Fourier transform, we have

$$C_1(s)e^{m(h_2+h_3)}-C_2(s)e^{-m(h_2+h_3)}=0,\tag{A.12}$$

$$D_1(s)e^{s(h_2+h_3)}-D_2(s)e^{-s^{s(h_2+h_3)}}=0,\tag{A.13}$$

$$\lambda_1A_2(s)e^{\lambda_1h_2}+\lambda_2A_3(s)e^{\lambda_2h_2}=m[C_1(s)e^{mh_2}-C_2(s)e^{-mh_2}],\tag{A.14}$$

$$A_2(s)e^{\lambda_1h_2}+A_3(s)e^{\lambda_2h_2}=C_1(s)e^{mh_2}+C_2(s)e^{-mh_2},\tag{A.15}$$

$$\gamma_1B_2(s)e^{\gamma_1h_2}+\gamma_2B_3(s)e^{\gamma_2h_2}=s\left[D_1(s)e^{sh_2}-D_2(s)e^{-sh_2}\right],\tag{A.16}$$

$$D_1(s)e^{sh_2}+D_2(s)e^{-sh_2}=B_2(s)e^{\gamma_1h_2}+B_3(s)e^{\gamma_2h_2}.\tag{A.17}$$

Solving Eqs. (36–37) and (A.12–A.17) with 10 unknown functions, we have

$$\begin{aligned}H_1(s)&=\frac{1-e^{2sh_3}}{1+e^{2sh_3}},\quad H_2(s)=\frac{1-e^{2mh_3}}{1+e^{2mh_3}},\\ Q_1(s)&=\frac{1}{\lambda_2}\frac{\lambda_2-sH_1(s)}{\lambda_1-sH_1(s)}e^{(\lambda_2-\lambda_1)h_2},\quad R_1(s)=\frac{1}{\gamma_2}\frac{\gamma_2-mH_2(s)}{\gamma_1-mH_2(s)}e^{(\gamma_2-\gamma_1)h_2},\\ A_1(s)&=A_2(s)+\frac{M(s)}{\lambda_1},\quad A_2(s)=-Q_1(s)M(s),\quad A_3(s)=\frac{M(s)}{\lambda_2},\end{aligned}$$

$$B_1(s) = B_2(s) + \frac{N(s)}{\gamma_1}, \quad B_2(s) = -R_1(s)N(s), \quad B_3(s) = \frac{N(s)}{\gamma_2},$$
$$C_1(s) = \frac{A_2(s)e^{\lambda_1 h_2} + A_3(s)e^{\lambda_2 h_2}}{1 + e^{2mh_3}} e^{-mh_2}, \quad C_2(s) = C_1(s)e^{2m(h_2+h_3)},$$
$$D_1(s) = \frac{\gamma_1 B_2(s)e^{\gamma_1 h_2} + \gamma_2 B_3(s)e^{\gamma_2 h_2}}{s(1 - e^{2sh_3})} e^{-h_2 s}, \quad D_2(s) = D_1(s)e^{2s(h_2+h_3)}.$$

Appendix C

$$Q(s) = 1 - \lambda_1 Q_1(s),\ R(s) = 1 - \gamma_1 R_1(s),\ F_1(s) = \frac{2\lambda_1\lambda_2}{s(\lambda_2 - \lambda_1)} Q(s),\ F_2(s) = \frac{2\gamma_1\gamma_2}{s(\gamma_2 - \lambda_1)} R(s).$$

References

1. Li, C., Weng, G.J.: Antiplane crack problem in functionally graded piezoelectric materials. ASME J. Appl. Mech. **69**, 481–488 (2002)
2. Chen, J., Liu, Z.X., Zou, Z.Z.: The central crack problem for a functionally graded piezoelectric strip. Int. J. Fract. **121**, 81–94 (2003)
3. Shin, J.W., Kim, T.U., Kim, S.C.: Dynamic characteristics of an eccentric crack in a functionally graded piezoelectric ceramic strip. J. Mech. Sci. Technol. **18**, 1582–1589 (2004)
4. Hu, K., Zhong, Z.: A moving mode-III crack in a functionally graded piezoelectric strip. Int. J. Mech. Mater. Des. **2**, 61–79 (2005)
5. Yong, H.D., Zhou, Y.H.: A mode III crack in a functionally graded piezoelectric strip bonded to two dissimilar piezoelectric half-planes. Compos. Struct. **79**, 404–410 (2007)
6. Jiang, L.Y.: The fracture behavior of functionally graded piezoelectric materials with dielectric cracks. Int. J. Fract. **149**, 87–104 (2008)
7. Shin, J.W., Kim, T.U., Kim, S.J., Hwang, I.H.: Dynamic propagation of a finite eccentric crack in a functionally graded piezoelectric ceramic strip. J. Mech. Sci. Technol. **23**, 1–7 (2009)
8. Shin, J.W., Lee, Y.S.: A moving interface crack between two dissimilar functionally graded piezoe-lectric layers under electromechanical loading. Int. J. Solids Struct. **47**, 2706–2713 (2010)
9. Li, X., Ding, S.H.: Periodically distributed parallel cracks in a functionally graded piezoelectric (FGP) strip bonded to a FGP substrate under static electromechanical load. Comput. Mater. Sci. **50**, 1477–1484 (2011)
10. Li, X., Long, Y.Y.: Thermal effect of functionally graded piezoelectric materials with crack by electric shock. Int. J. Mech. Res. **1**, 1–7 (2012)
11. Zhou, Y.T., Lee, K.Y.: Investigation of frictional sliding contact problems of triangular and cylindrical punches on monoclinic piezoelectric materials. Mech. Mater. **69**, 237–250 (2014)
12. Shen, S.P., Kuang, Z.B.: Wave scattering from an interface crack in laminated anisotropic media. Mech. Res. Commun. **25**, 509–517 (1998)
13. Wang, X.D., Meguid, S.A.: Modeling and analysis of the dynamic behavior of piezoelectric materials containing interacting cracks. Mech. Mater. **32**, 723–737 (2000)
14. Gu, B., Yu, S.W., Feng, X.Q.: Elastic wave scattering by an interface crack between a piezoelectric layer and elastic substrate. Int. J. Fract. **116**, L29–L34 (2002)
15. Ueda, S.: Diffraction of antiplane shear waves in a piezoelectric laminate with a vertical crack. Euro. J. Mech. A Solids **22**, 413–422 (2003)
16. Zhou, Z.G., Wang, B.: The scattering of harmonic anti-plane shear waves by an interface crack in magneto-electro-elastic composites. Appl. Math. Mech. **26**, 17–26 (2005)
17. Ma, L., Nie, W., Wu, L.Z., Guo, L.C.: Scattering of anti-plane stress waves by a crack in a non-homogeneous orthotropic medium. Compos. Struct. **79**, 174–179 (2007)
18. Li, X., Liu, J.Q.: Scattering of the SH wave from a crack in a piezoelectric substrate bonded to a half-space of functionally graded materials. Acta Mech. **208**, 299–308 (2009)
19. Huang, Y., Li, X.F.: Shear waves guided by the imperfect interface of two magnetoelectric materials. Ultrasonics **50**, 750–757 (2010)
20. Zhao, J., Pan, Y., Zhong, Z.: Theoretical study of shear horizontal wave propagation in periodically layered piezoelectric structure. J. Appl. Phys. **111**, 064906-1–064906-11 (2012)
21. Singh, B.M., Rokne, J.: Propagation of SH waves in layered functionally gradient piezoelectric–piezomagnetic structures. Philos. Mag. **93**, 1690–1700 (2013)
22. Yang, J., Li, X.: Scattering of the SH wave by a crack magneto-electro-elastic material substrate bonded to piezoelectric material. Theor. Appl. Fract. Mech. **74**, 109–115 (2014)
23. Hao, T.H., Shen, Z.Y.: A new electric boundary condition of electric fracture mechanics and its applications. Eng. Fract. Mech. **47**, 793–802 (1994)
24. Kwon, S.M.: On the dynamic propagation of an anti-plane shear crack in a functionally graded piezoelectric strip. Acta Mech. **167**, 73–89 (2004)

25. Sun, J.L., Zhou, Z.G., Wang, B.: Dynamic behavior of a crack in a functionally graded piezoelectric strip bonded to two dissimilar half piezoelectric material planes. Acta Mech. **176**, 4–60 (2005)
26. Copson, E.T.: On certain dual integral equations. Proc. Glasg. Math. Assoc. **5**, 21–24 (1961)
27. Narita, F., Shindo, Y.: Dynamic anti-plane shear of a cracked piezoelectric ceramic. Theor. Appl. Fract. Mech. **29**, 169–180 (1998)